JBC RESEARCH ARTICLE

Pirh2-dependent DNA damage in neurons induced by the G-quadruplex ligand pyridostatin

Received for publication, January 31, 2023, and in revised form, July 28, 2023 Published, Papers in Press, August 12, 2023,
https://doi.org/10.1016/j.jbc.2023.105157

Rocio Diaz Escarcega[1], Abhijeet A. Patil[1], Jose F. Moruno-Manchon[1], Akihiko Urayama[1], Sean P. Marrelli[1], Nayun Kim[2], David Monchaud[3], Louise D. McCullough[1,4], and Andrey S. Tsvetkov[1,4,5,*]

From the [1]Department of Neurology, and [2]Department of Microbiology and Molecular Genetics, The University of Texas McGovern Medical School, Houston, Texas, USA; [3]Institut de Chimie Moléculaire (ICMUB), UBFC Dijon, CNRS UMR6302, Dijon, France; [4]The University of Texas Graduate School of Biomedical Sciences, Houston, Texas, USA; [5]UTHealth Consortium on Aging, The University of Texas McGovern Medical School, Houston, Texas, USA

Reviewed by members of the JBC Editorial Board. Edited by Patrick Sung

Noncanonical base pairing between four guanines (G) within single-stranded G-rich sequences leads to formation of a G-quartet. Self-stacking of G-quartets results in a columnar four-stranded DNA structure known as the G-quadruplex (G4 or G4-DNA). In cancer cells, G4-DNA regulates multiple DNA-dependent processes, including transcription, replication, and telomere function. How G4s function in neurons is poorly understood. Here, we performed a genome-wide gene expression analysis (RNA-Seq) to identify genes modulated by a G4-DNA ligand, pyridostatin (PDS), in primary cultured neurons. PDS promotes stabilization of G4 structures, thus allowing us to define genes directly or indirectly responsive to G4 regulation. We found that 901 genes were differentially expressed in neurons treated with PDS out of a total of 18,745 genes with measured expression. Of these, 505 genes were downregulated and 396 genes were upregulated and included gene networks regulating p53 signaling, the immune response, learning and memory, and cellular senescence. Within the p53 network, the E3 ubiquitin ligase *Pirh2* (*Rchy1*), a modulator of DNA damage responses, was upregulated by PDS. Ectopically overexpressing Pirh2 promoted the formation of DNA double-strand breaks, suggesting a new DNA damage mechanism in neurons that is regulated by G4 stabilization. Pirh2 downregulated DDX21, an RNA helicase that unfolds G4-RNA and R-loops. Finally, we demonstrated that Pirh2 increased G4-DNA levels in the neuronal nucleolus. Our data reveal the genes that are responsive to PDS treatment and suggest similar transcriptional regulation by endogenous G4-DNA ligands. They also connect G4-dependent regulation of transcription and DNA damage mechanisms in neuronal cells.

The G-quadruplex (G4) is a four-stranded higher-order nucleic acid structure that folds from single-stranded guanine (G)-rich DNA or RNA sequences. Intramolecular folding of G-enriched sequences is promoted by the self-association of four Gs to form G-quartets, which are then stacked on top of each other. Physiological cations, such as K^+ or Na^+, promote G4-DNA and G4-RNA formation and stabilization by decreasing the electron density within the central stem of the G4 structure that results from the presence of inwardly pointing carbonyl groups of Gs (four carbonyls per a G-quartet). G4-DNA and G4-RNA are thermodynamically highly stable structures with fast and reversible formation kinetics (1) and are functionally modulated in cells by chaperones and helicases (2–4). All these features make G4s ideal genetic levers to control DNA- and RNA-dependent processes, including gene expression at the transcriptional and translational levels (5, 6).

Putative G4-forming sequences (QFSes) were identified in the human genome by both *in silico* (7) and genome-wide (*e.g.*, G4-Seq, G4 chromatin immunoprecipitation-Seq) or transcriptome-wide methods (*e.g.*, rG4-Seq, G4RP-Seq) (8). QFSes are often located in gene promoters (9), near the replication start sites (10), and in mitochondrial DNA (11). G4 chromatin immunoprecipitation-Seq demonstrated that G4-DNA forms at nucleosome-depleted and transcriptionally active sites (12), thus functionally linking G4s to active DNA-dependent processes (8). Analyses of "active" G4-DNA structures revealed that G4 landscapes differ between cell types (13, 14), and these G4 landscapes are regulated by G4-DNA-binding proteins and G4-DNA helicases (3, 4). We previously showed that the predominant cells in the brain—neurons, astrocytes, and microglia—basally exhibit different G4 landscapes (15).

Many small-molecule G4-DNA ligands that bind to G4s have been discovered over the last decade. Pyridostatin (PDS), the most studied G4 ligand, is an efficient G4-DNA stabilizer and a potential chemotherapy agent as it promotes DNA double-strand breaks (DSBs) at G4 sites (16–19). Intriguingly, in cancer cells, PDS activates a number of innate immune genes, suggesting that G4 ligands may act as immunomodulators (20). G4 ligands have been extensively studied in yeast and cancer cells, providing insights into G4 functions in these cell types. However, little is known about how G4 ligands modulate DNA-based mechanisms in many other cell types, such as postmitotic neurons.

Genome integrity is critical for neurons, and thus, these cells devote substantial resources to minimize genomic instability

* For correspondence: Andrey S. Tsvetkov, andrey.s.tsvetkov@uth.tmc.edu.

(21). DNA damage and repair occur in neurons during normal physiologic activity (22). However, as neuronal cells age, the DNA repair machinery (DNA damage response [DDR]) is less efficient, leading to genomic instability and cellular dysfunction (23). DNA damage is associated with many age-associated neurodegenerative diseases, including Alzheimer's disease, Parkinson's disease, amyotrophic lateral sclerosis, and Huntington's disease (24, 25). G4-DNA is also involved in DNA recombination, deletion, and gross chromosomal rearrangements (26–30). Overly stabilized G4-DNA structures act as physical barriers for polymerases, leading to DNA damage *via* transcription-coupled repair poisoning (31) and/or Top2 trapping at G4 sites (17, 18, 32). Various G4-regulating proteins suppress G4-associated genomic instability in yeast (28, 33–35) and cancer cells (36, 37). We reported that aged mouse brains contain higher levels of G4-DNA than young brains (38), and that stabilizing G4-DNA by PDS in neuronal cells contributes to genomic instability (39). However, the molecular mechanisms of G4-mediated genomic instability in neurons are still poorly understood (40).

In this study, we performed genome-wide gene expression analysis (RNA-Seq) to identify genes modulated by PDS in primary cultured neurons. We found that 901 genes were differentially expressed in neurons treated with PDS out of a total of 18,745 genes with measured expression. Our findings indicate that G4s represent an important mechanism of transcriptional regulation in neuronal cells, involving a network of genes regulating p53 signaling, immune response, learning and memory, cellular senescence, and others. We also found that the E3 ubiquitin ligase *Pirh2* (*Rchy1*), which promotes the degradation of DDR proteins, was upregulated by PDS. Interestingly, ectopically overexpressing Pirh2 promotes the formation of DNA DSBs in neurons. We discovered that Pirh2 downregulates DDX21, an RNA helicase that unfolds G4-RNA and R-loops that form cotranscriptionally (41, 42). We also found that Pirh2 promotes G4-DNA formation in the neuronal nucleolus. Our findings indicate that G4s are an important mechanism for modulating gene expression and DDRs in neurons.

Results

PDS alters transcription in cultured primary neurons

Previously, we reported that in neurons, stabilizing G4s with PDS promotes changes in chromatin structure (15) and reduces transcription of several genes that contain G4-DNA motifs (15, 38, 39). Therefore, we decided to investigate whether and how stabilizing G4-DNA with PDS would affect the whole transcriptome expression in primary cultured neurons. We hypothesized that comparing transcription in neurons treated with PDS or vehicle would reveal physiologically relevant G4-dependent molecular mechanisms. Primary mouse cortical neurons were cultured for 14 days (14 days *in vitro* [DIV]) until they were synaptically established. Neurons were then treated with PDS or vehicle (overnight) and analyzed by RNA-Seq. With QIAGEN RNA-Seq, we found that high-quality data were obtained for all samples (Supplemental Data 1 and 2). Principal component analysis (PCA) of RNA-Seq results revealed that the differences between control and PDS-treated samples were well pronounced (Fig. 1*A*). PDS-treated samples showed greater variability in clustering compared with control, which is commonly observed in RNA-Seq analyses. By RNA-Seq, 901 genes were differentially expressed in neurons treated with PDS out of a total of 18,745 genes with measured expression. Of those, 505 genes were downregulated and 396 genes were upregulated (Fig. 1, *B–E*). The upregulated genes tended to have a higher fold change compared with downregulated genes (Fig. 1, *C–E*); however, the number of genes downregulated was higher (Fig. 1, *B* and *C*). Since PCA of RNA-Seq data demonstrated separation of one individual sample in the PDS group, we removed the separated dataset and reran our analyses, which did not considerably affect the results (Fig. S1, *A* and *B*). With that analysis, 517 genes were downregulated and 394 genes were upregulated (Fig. S1, *A* and *B*), indicating that variability in the PDS cohort did not significantly alter the outcome data. Overall, we discovered that, similar to a previous study in cancer cells (20), PDS treatment results in transcriptional changes, both positive and negative.

PDS alters neuron-specific and neuron-nonspecific gene networks

RNA-Seq data were analyzed in the context of pathways obtained from the Kyoto Encyclopedia of Genes and Genomes (KEGG) database (43, 44) and gene ontologies from the Gene Ontology (GO) Consortium database (45). The underlying pathway topologies, including genes and their directional interactions, were obtained from the KEGG database using iPathwayGuide (Advaita Bioinformatics). In our analyses, 1583 GO terms were found to be significantly enriched in PDS-treated samples. Among them, neuron-specific and neuron-nonspecific networks were enriched (Fig. 2, *A–C*). For example, nervous system development, neuronal differentiation, neurogenesis, and learning and memory networks were enriched. Cellular senescence, cell death, re-entry into mitotic cell cycle, DDR, and negative and positive regulation of autophagosome networks were affected (Fig. 2, *A* and *B*). Immune response genes were also affected by PDS, which was also seen in a study with cancer cells (20). Intriguingly, the positive regulation of amyloid precursor protein network was affected by PDS (Fig. 2*A*). Our data indicate that PDS induces neuron-specific and neuron-nonspecific transcriptional changes in primary cultured neurons.

The p53 pathway is one of the most affected by PDS

One of the most affected pathways was the p53 pathway (46) (KEGG: 04115) with 17 genes dysregulated (16 genes upregulated, one downregulated, Fig. 3, *A–C*). Among upregulated genes was the *Pirh2* (*Rchy1*) gene (Fig. 3, *C* and *D*). Its corresponding protein interacts with G4 helicases in cancer cells (47), suggesting an interesting connection between PDS, Pirh2, and G4 helicases. With quantitative PCR (qPCR), we confirmed that PDS indeed upregulates the *Pirh2* gene in

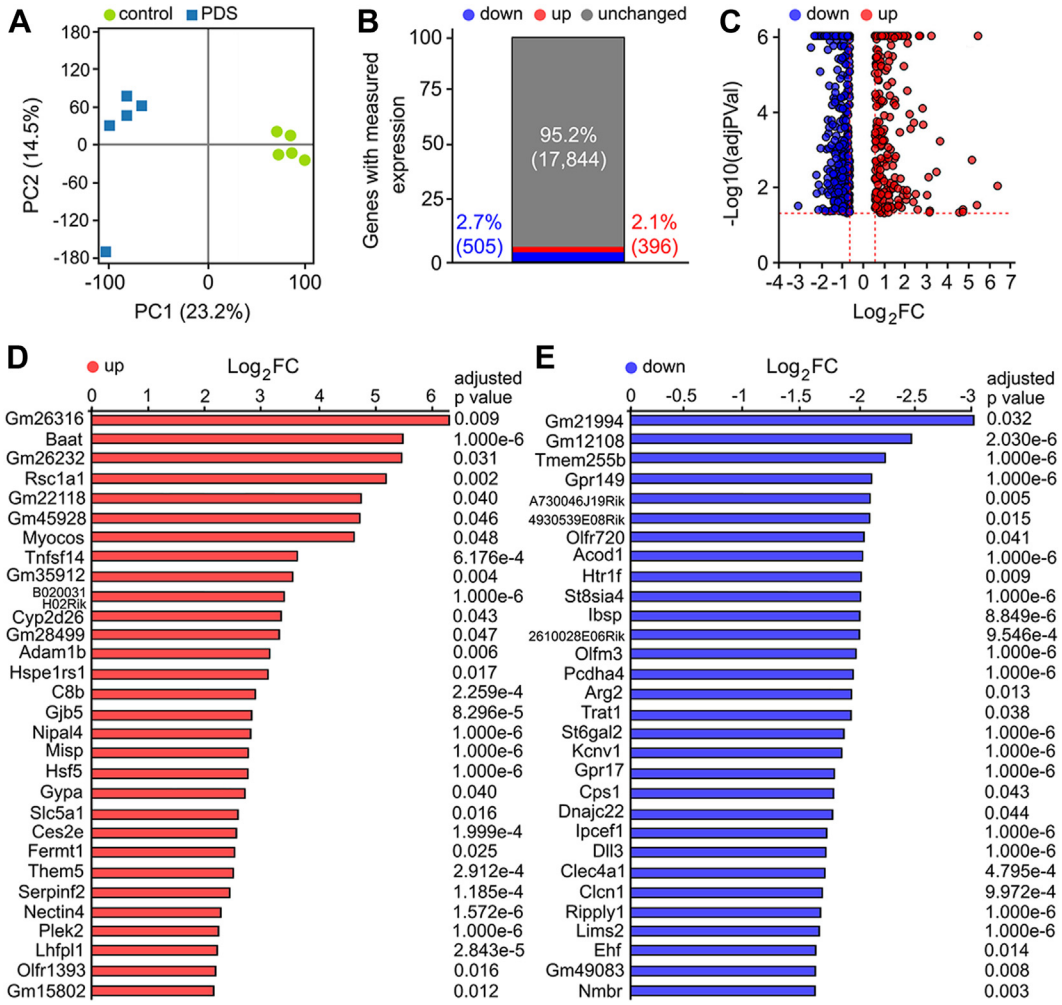

Figure 1. Pyridostatin (PDS) alters transcription in cultured primary neurons. *A*, principal component analysis (PCA) is used to define RNA-Seq profiles. PCA of RNA-Seq data for five vehicle-treated and five PDS-treated (2 μM, overnight) samples is shown. Each *dot* represents an individual sample. The percentage values refer to the percentage of total variance associated with each component. *Green*: control, *blue*: PDS. *B*, 901 differentially expressed (DE) genes were identified out of a total of 18,745 genes with measured expression. The thresholds used to select the DE genes were 0.6 for expression change and 0.05 for significance. *C*, the volcano plot illustrates 901 DE genes. The significance is represented in terms of the negative log (base 10) of the *p* value, so that more significant genes are plotted higher on the *y*-axis. The *dotted lines* representing the thresholds used to select the DE genes are 0.6 for expression change and 0.05 for significance. The upregulated genes are shown in *red*, and the downregulated genes are shown in *blue*. *D*, the top 30 upregulated genes (*red*) and (*E*), the top 30 downregulated genes (*blue*) illustrate a diversity of altered genes.

cultured primary neurons (Fig. 3*E*). Since PCA of RNA-Seq data showed separation of one individual sample in the PDS group, we again removed the separated dataset and performed our iPathwayGuide analyses. Removing the dataset did not have a considerable effect on our findings (Fig. S2). In particular, the same 16 genes, including *Pirh2*, were upregulated and one gene was downregulated with small changes in the *p* and fold-change values (Fig. S2). Overall, the p53 signaling pathway may be affected by PDS-induced DNA damage and/or altered transcription of specific genes, triggering positive and negative feedback loops, which enhance and/or attenuate the p53 protein and integrate its functions with other signaling pathways.

We then used the QFS mapper (QGRS) to computationally analyze the *Pirh2* gene and its promoter in several species for the presence of putative G4-DNA motifs (Fig. S3). In *Homo sapiens* and *Mus musculus*, *Pirh2* has two putative G4-DNA sequences, and its promoter has none. In *Rattus norvegicus*, *Pirh2* and its promoter form have no QFSes (Fig. S3). A recent study generated whole-genome experimental maps of G4-DNA in multiple species (9). In agreement with our computational data, the *Pirh2* promoter was found to contain no G4-DNA (9), indicating that the effect of PDS on Pirh2 might be indirect rather than direct.

PDS effects on neuronal transcription depend on neuronal development stage

While analyzing our data from 14 DIV neurons treated with PDS, we noticed differences compared with our earlier data generated with four DIV neurons (39). In synaptically developed 14 DIV neurons, the most affected pathway was the neuroactive ligand–receptor interaction pathway (KEGG: 04080) that included synaptic receptor genes (Fig. 3*A*). Many of these genes were not expressed in cultured neurons soon after plating, and thus, the data generated with freshly plated neurons would be expected to be different.

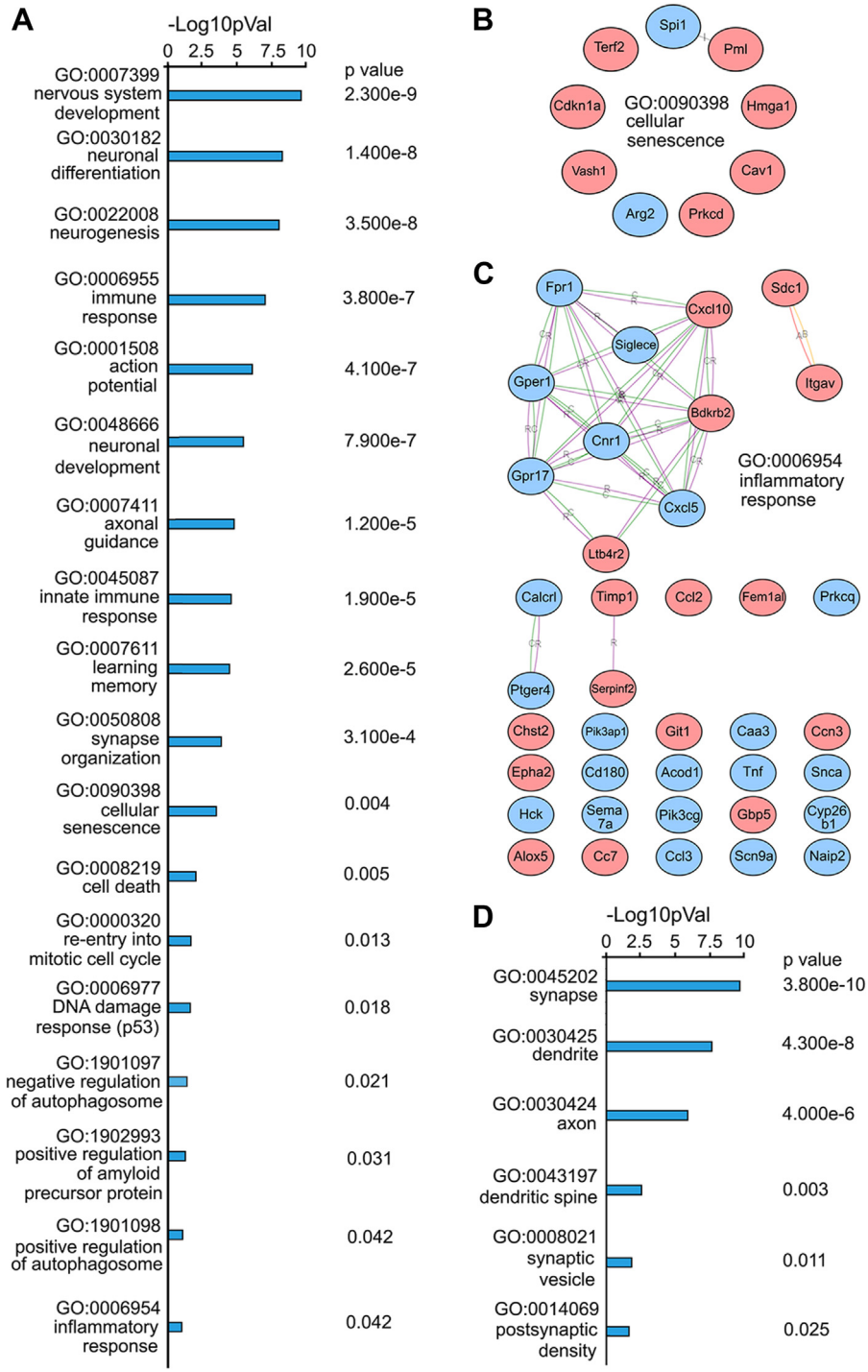

Figure 2. Biological processes affected by pyridostatin (PDS) in cultured primary neurons. *A*, Gene Ontology (GO) terms illustrate that PDS (2 μM, overnight) affects various neuron-specific and neuron-nonspecific pathways. *B*, an example of cell senescence genes (GO:0090398) affected by PDS (2 μM, overnight). *C*, an example of inflammatory response genes (GO:0006954) affected by PDS (2 μM, overnight). *D*, GO terms for cellular components illustrate enrichment for neuronal genes altered by PDS (2 μM, overnight).

In our earlier four DIV data generated with RT–qPCR, we showed that transcription of the *Atg7* gene was diminished by PDS; however, the current 14 DIV data show that *Atg7* was not affected. Transcription of the *Brca1* gene was reduced by PDS in four DIV neurons (shown by RT–qPCR), but the current 14 DIV data show that *Brca1* was not affected. We, therefore, tested if there was a difference in the expression of *Atg7* and *Brca1* in 14 DIV and four DIV neurons measured by PCR using *Tbp* as the internal control that we discovered earlier (39). The *Tbp* gene was not affected by PDS in the current RNA-Seq dataset either (Supplemental Data 1). About 14 DIV and four DIV neurons were treated with PDS, and then mRNA was extracted and analyzed (Fig. S4). Levels of both *Atg7* and *Brca1* went down in four DIV neurons treated with PDS, whereas 14 DIV neuronal cells only exhibited a nonsignificant trend (Fig. S4). Interestingly, PDS robustly upregulated *Pirh2*

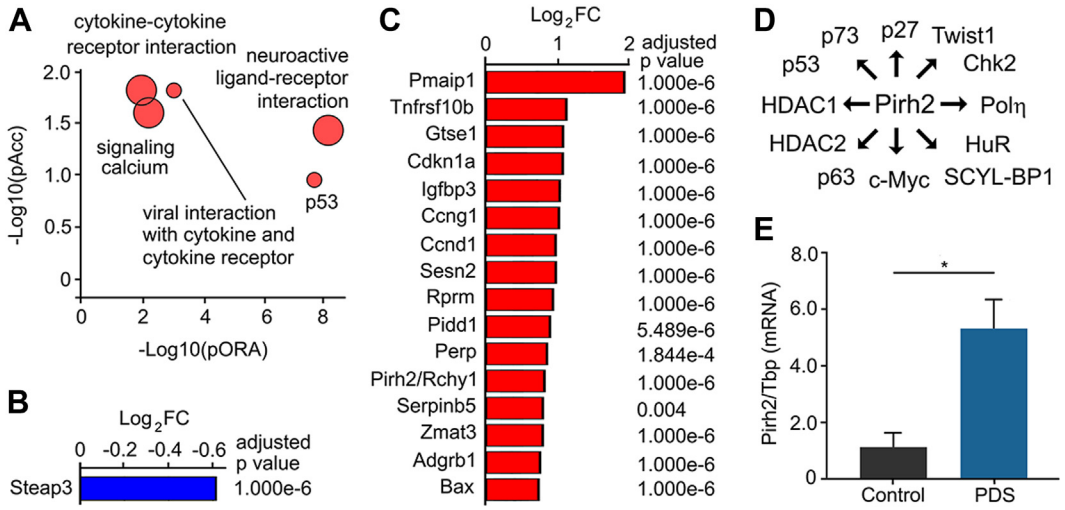

Figure 3. The p53 pathway is one of the most affected by pyridostatin (PDS) in cultured primary neurons. *A*, pathway perturbation *versus* over-representation shows one of the most affected pathways. Over-representation is shown on the *x*-axis (pORA), and the total pathway accumulation is shown on the *y*-axis (pAcc). Each pathway is represented by a single dot, and the size of each dot is proportional to the size of the pathway it represents. The second most affected pathway is the p53 pathway (KEGG: 04115), $p = 2.151 \times 10^{-6}$. *B*, Steap3, a gene from the p53 pathway, is downregulated by PDS (2 μM, overnight). *C*, 16 genes from the p53 pathway are upregulated by PDS (2 μM, overnight). Note that among upregulated genes is the Pirh2 (Rchy1) gene. *D*, Pirh2, an E3 ubiquitin ligase, induces the degradation of a variety of proteins. *E*, primary neurons (14 DIV) were treated with a vehicle (control) or with 2 μM PDS overnight. The expression of Pirh2 was determined by quantitative RT–PCR relative to Tbp. $p = 0.0184$ (*t* test). Results were pooled from three independent experiments. DIV, days *in vitro*; KEGG, Kyoto Encyclopedia of Genes and Genomes.

in both 14 DIV and four DIV neurons, indicating that the p53 pathway is altered by PDS in developed and freshly plated cells. We conclude that freshly plated developing neurons and synaptically established cells respond to PDS differently, at least in part, likely reflecting developmental differences in transcriptional activity. These results implicate PDS-mediated changes in neuronal transcriptional activity rather than a DNA damage–mediated pathway.

Pirh2 is enriched in the neuronal nucleolus

Pirh2 localizes to the cytoplasm, as well as to intranuclear foci in cancer cells, although the nature of those foci was not clear (48). Pirh2 interacts with and ubiquitinates a number of proteins in the nucleus and in the cytoplasm (49–52). To eliminate any cytoplasmic contribution to the nuclear mechanisms that we aimed to study, we cloned a blue fluorescent protein-tagged construct with a nuclear localization sequence (NLS) to specifically targeted Pirh2 to the nucleus (NLS-BFP [blue fluorescent protein]-Pirh2; referred as to BFP-Pirh2 hereafter). Primary cortical neurons were transfected with BFP-Pirh2, fixed, and stained with antibodies raised against MAP2c and a nuclear dye (SYTOX). Pirh2 was concentrated in the nucleus and enriched in intranuclear foci (Fig. 4*A*). Intriguingly, BFP-Pirh2 often formed ring-like structures within the neuronal nucleus (Fig. 4*A*), indicating that treatment of BFP-Pirh2-expressing cells with PDS promoted condensation of foci (Fig. 4, *A*–*C*).

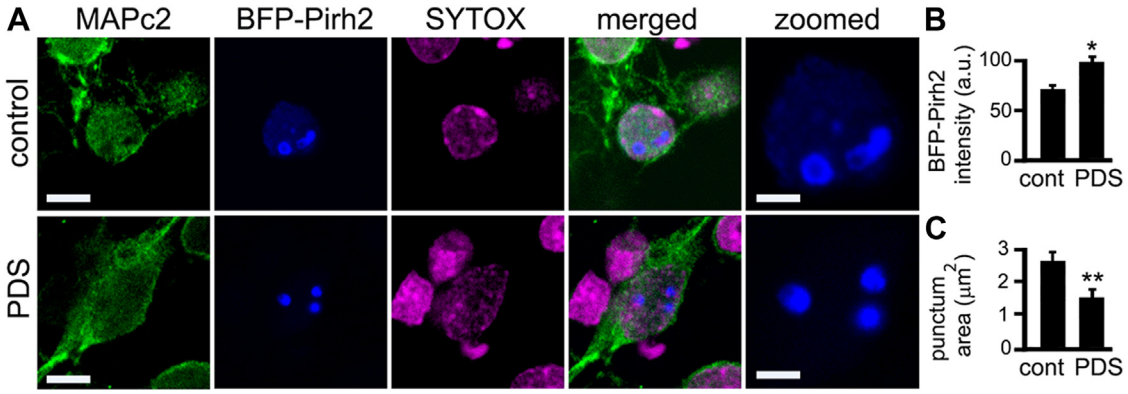

Figure 4. Pirh2 forms intranuclear foci in cultured primary neurons. *A*, primary cortical neurons were transfected with BFP-Pirh2 and treated with a vehicle or pyridostatin (PDS). Cells were fixed and stained with antibodies raised against MAP2c and the SYTOX nuclear dye and imaged with a confocal microscope. Note BFP-Pirh2 is enriched in the intranuclear punctuate foci with a ring-like structure. Also note that PDS alters the appearance of the intranuclear punctuate foci. Scale bar represents 5 μm. The nuclei in the blue channel are zoomed in to demonstrate that PDS alters BFP-Pirh2-positive structures. Scale bar represents 2 μm. *B*, the intensity of BFP-Pirh2-positive foci was estimated by measuring the BFP signal in the punctum area from (*A*) $p = 0.02$ (*t* test). *C*, the area of BFP-Pirh2-positive foci was estimated by measuring the BFP signal from (*A*) $p = 0.0056$ (*t* test), 34 neurons were analyzed from three independent experiments in (*B*) and (*C*). a.u., arbitrary unit; BFP, blue fluorescent protein.

There are several subdomains in the nucleus, including promyelocytic leukemia (PML) bodies (53) and the nucleoli (54). First, we tested if BFP-Pirh2-positive structures were in the PML bodies. Primary cortical neurons were transfected with PML-GFP and BFP-Pirh2, fixed, stained with an antibody against MAP2c, and analyzed with confocal microscopy. We discovered that BFP-Pirh2-positive structures and PML bodies were distinct intranuclear structures, although some PML bodies were in close proximity to the Pirh2-positive foci (Fig. 5, *A*–*C*).

We then tested if BFP-Pirh2-positive structures were the nucleoli. Primary cultured neurons were transfected with BFP-Pirh2, fixed, and stained with an antibody against nucleolin. We discovered that BFP-Pirh2-positive signal indeed colocalized with the nucleoli (Fig. 5, *D* and *E*). We conclude that, in the neuronal nucleus, Pirh2 was enriched in the nucleoli, which often communicate with the PML bodies. The nucleolus and PML bodies communicate and exchange protein factors with each other especially when the cell is stressed (*e.g.*, during DNA damage) (55).

Elevated nuclear Pirh2 promotes ubiquitination, DNA damage, and neurodegeneration

We next questioned whether ectopically expressed BFP-Pirh2 promotes protein ubiquitination in our neuronal system, as the endogenous Pirh2 does (56). We hypothesized that the nuclear-targeted BFP-Pirh2 construct promotes protein ubiquitination in our neuronal system. Primary cortical neurons were cotransfected with either mApple and BFP or with mApple and BFP-Pirh2 construct. Neurons were fixed 24 h after transfection and stained with a ubiquitin antibody. Indeed, we discovered that BFP-Pirh2-overexpressing neurons exhibited higher ubiquitin levels than control neurons (Fig. 6, *A*–*C*). Importantly, BFP-Pirh2-positive foci were positive for ubiquitin (Fig. 6, *A*–*C*). We conclude that the BFP-Pirh2 construct is basally active and ubiquitinates substrates in the neuronal nucleus.

Since Pirh2 downregulates DDR proteins (56), we sought to determine if overexpressed Pirh2 promotes DNA damage in neurons. Cultured primary neurons were transfected with the BFP-Pirh2 construct or BFP as a control, fixed, and stained with antibodies against γH2AX, a marker of DSBs (39, 57). Neurons transfected with BFP-Pirh2 exhibited increased fluorescence intensity and higher puncta index of the γH2AX marker (Fig. 7, *A* and *B*). Critically, the γH2AX foci primarily were localized to the BFP-Pirh2-positive foci (Fig. 7*A*).

As an alternative method to study DNA damage in living neurons, we also used the Apple-53BP1trunc construct–based method (58) that we recently adapted to our neuronal system

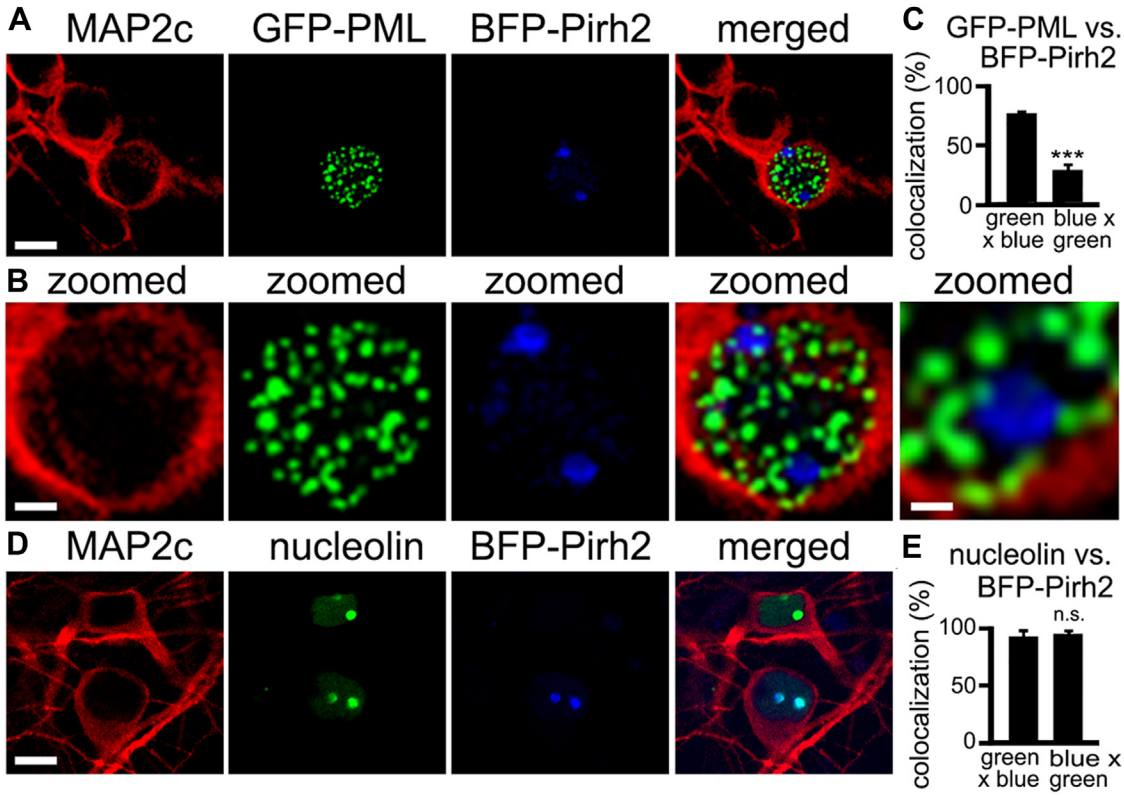

Figure 5. Pirh2 is enriched in the neuronal nucleolus. *A*, primary cortical neurons were transfected with GFP-PML and BFP-Pirh2, fixed, and stained with antibodies against MAP2c, and imaged with a confocal microscope. Scale bar represents 5 μm. *B*, the nucleus from (*A*) is zoomed in to demonstrate that PML-positive and Pirh2-positive foci are separate structures. Note that BFP-Pirh2-positive foci are ring-like structures. Scale bar represents 2 μm. The *right panel* is zoomed in from the *left panels* to demonstrate that BFP-Pirh2-positive structures and PML bodies are distinct intranuclear structures. Scale bar represents 0.2 μm. *C*, colocalization of BFP-Pirh2 and GFP-PML was measured from (*A*). $p = 0.0002$ (*t* test), 80 neurons were analyzed. *D*, primary cortical neurons were transfected with NLS-BFP-Pirh2, fixed, and stained with antibodies against MAP2c and nucleolin, and imaged with a confocal microscope. Note that NLS-BFP-Pirh2 and nucleolin colocalize. Scale bar represents 5 μm. *E*, colocalization of BFP-Pirh2 and nucleolin was measured from (*D*). n.s. ($p = 0.27$, *t* test), 80 neurons were analyzed from three experiments. BFP, blue fluorescent protein; NLS, nuclear localization sequence; ns, nonsignificant; PML, promyelocytic leukemia.

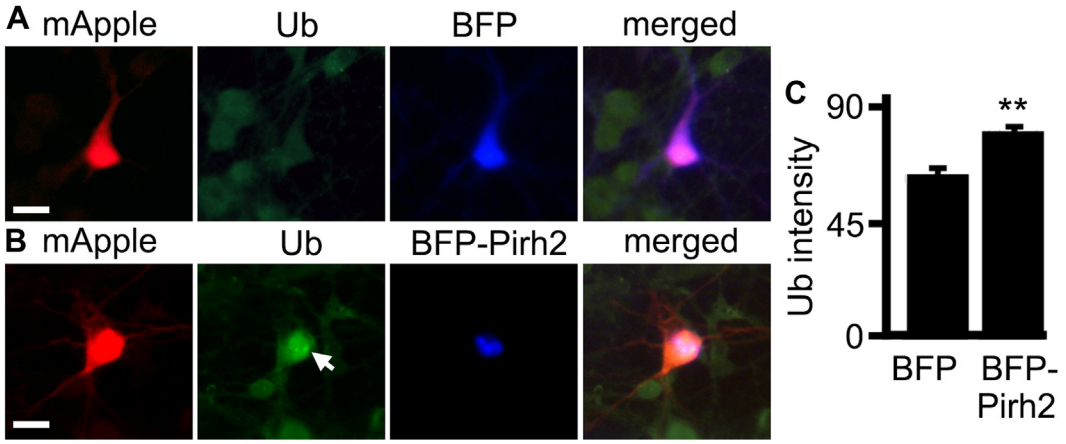

Figure 6. Pirh2 promotes ubiquitination in the neuronal nucleus. *A*, primary cortical neurons were cotransfected with mApple and BFP. Cells were fixed 24 h after transfection, stained with antibodies against ubiquitin (*green*), and imaged. Scale bar represents 10 μm. *B*, primary cortical neurons were cotransfected with mApple and BFP-Pirh2. Cells were fixed 24 h after transfection, stained with antibodies against ubiquitin (*green*), and imaged. Note *green puncta* in the nucleus of the neuron that expresses BFP-Pirh2 (depicted with *arrow*). Scale bar represents 10 μm. *C*, analyses of ubiquitin fluorescence form (*A*). $p = 0.0096$ (*t* test), 1582 BFP- and 1459 BFP-Pirh2-transfected neurons were analyzed from four experiments. BFP, blue fluorescent protein.

(39). The 53BP1trunc construct has no DNA repair ability (53BP1 being truncated), but it still binds to the DNA DSB sites. Having the red fluorescent protein mApple fused to the 53BP1trunc construct makes the Apple-53BP1trunc chimera a useful DNA DSB reporter in living cells (58). Primary neurons were cotransfected with Apple-53BP1trunc, GFP, and BFP, as control, or with Apple-53BP1trunc, GFP, and BFP-Pirh2. Neurons were imaged 24 and 36 h after transfection, and Apple-53BP1trunc's distribution was analyzed in the individual neurons. We discovered that BFP-Pirh2-overexpressing neurons exhibited higher levels of DNA damage than control neurons (Fig. 7, *C* and *D*). These data indicate that elevated Pirh2 promotes the formation of DNA DSBs in neurons.

DNA DSBs are the most dangerous of the many types of DNA damage as entire fragments of DNA can be lost if the DNA is not effectively and correctly repaired, and their accumulation eventually leads to cell death. To determine whether elevated Pirh2 is neurotoxic, primary neurons were cotransfected with GFP (a morphology and viability marker) and BFP or with GFP and BFP-Pirh2 and longitudinally imaged at 24 h intervals (59). Neurons transfected with the control GFP/BFP did not exhibit neurotoxicity, whereas GFP/BFP-Pirh2-transfected neurons degenerated, indicating the neurotoxicity of elevated Pirh2 (Fig. 7, *E* and *F*). In parallel, BFP- and BFP-Pirh2-expressing neurons were stained for annexin V, a marker of apoptotic cells. BFP-Pirh2-expressing neurons showed significantly higher signal for annexin V compared with BFP-expressing control neurons, corroborating our aforementioned finding of the neurotoxic potential of Pirh2 (Fig. S5).

Pirh2 downregulates DDX21 and increases nucleolar G4-DNA levels in neurons

A recent study showed that, in cancer cells, Pirh2 interacts with the nucleolar RNA helicase DDX21 (47), which resolves G4-RNA (60, 61) and R-loops that cotranscriptionally form with G4s (62). We hypothesized that Pirh2 downregulates DDX21, leading to increased formation of either R-loops, G4s, or both, and thereby results in structure-dependent DSBs (63) (as observed in Fig. 7, *A* and *B*).

First, we confirmed that DDX21 is a nucleolar protein in neurons. Cultured cortical neurons were transfected with the DDX21-NeonGreen construct and stained with an antibody raised against nucleolin. We found that DDX21-NeonGreen was enriched in the neuronal nucleolus (Fig. 8*A*). Intriguingly, unlike nucleolin that was enriched in the ring-like granular component of the nucleolus, DDX21-NeonGreen was enriched in the dense fibrillar component of the nucleolus (Fig. 8, *B* and *C*), where ribosomal DNA (rDNA) and rRNA are located (Fig. 8*B*). PDS promotes nucleolar condensation, and colocalization of the DDX21-NeonGreen and nucleolin signals increases (Fig. 8, *B* and *C*).

We then tested whether elevated Pirh2 affects the levels of DDX21 in the neuronal nucleolus. The first cohort of neurons was transfected with either NeonGreen and BFP or NeonGreen and BFP-Pirh2, and the levels of endogenous DDX21 were analyzed with immunocytochemistry (Fig. 8, *D* and *E*). We found that Pirh2 promoted downregulation of endogenous DDX21 in the nucleolus, likely contributing to DNA damage in neuronal cells. Importantly, PDS does not affect transcription of the *Ddx21* gene (Supplemental Data 1; LogFC = 0.127, $p = 0.143$). These data indicate that Pirh2 plays a role in regulating genomic stability by modulating levels of the DDX21 protein that prevents DNA damage in neurons.

Finally, we tested if elevated Pirh2 affects G4-DNA levels in the nucleolus. Neurons were transfected with BFP and the G4-DNA reporter G4P-mScarlet (64) or with BFP-Pirh2 and G4P-mScarlet, fixed, and stained with an antibody against MAP2c and SYTOX (Fig. 9*A*). The intensity of G4P-mScarlet fluorescence was analyzed in BFP-Pirh2-positive puncta. Pirh2 promotes G4-DNA formation in the neuronal nucleolus (Fig. 9, *A* and *B*). Our results revealed a novel Pirh2-, DDX21-, and G4-DNA-dependent mechanism of DNA damage in neurons.

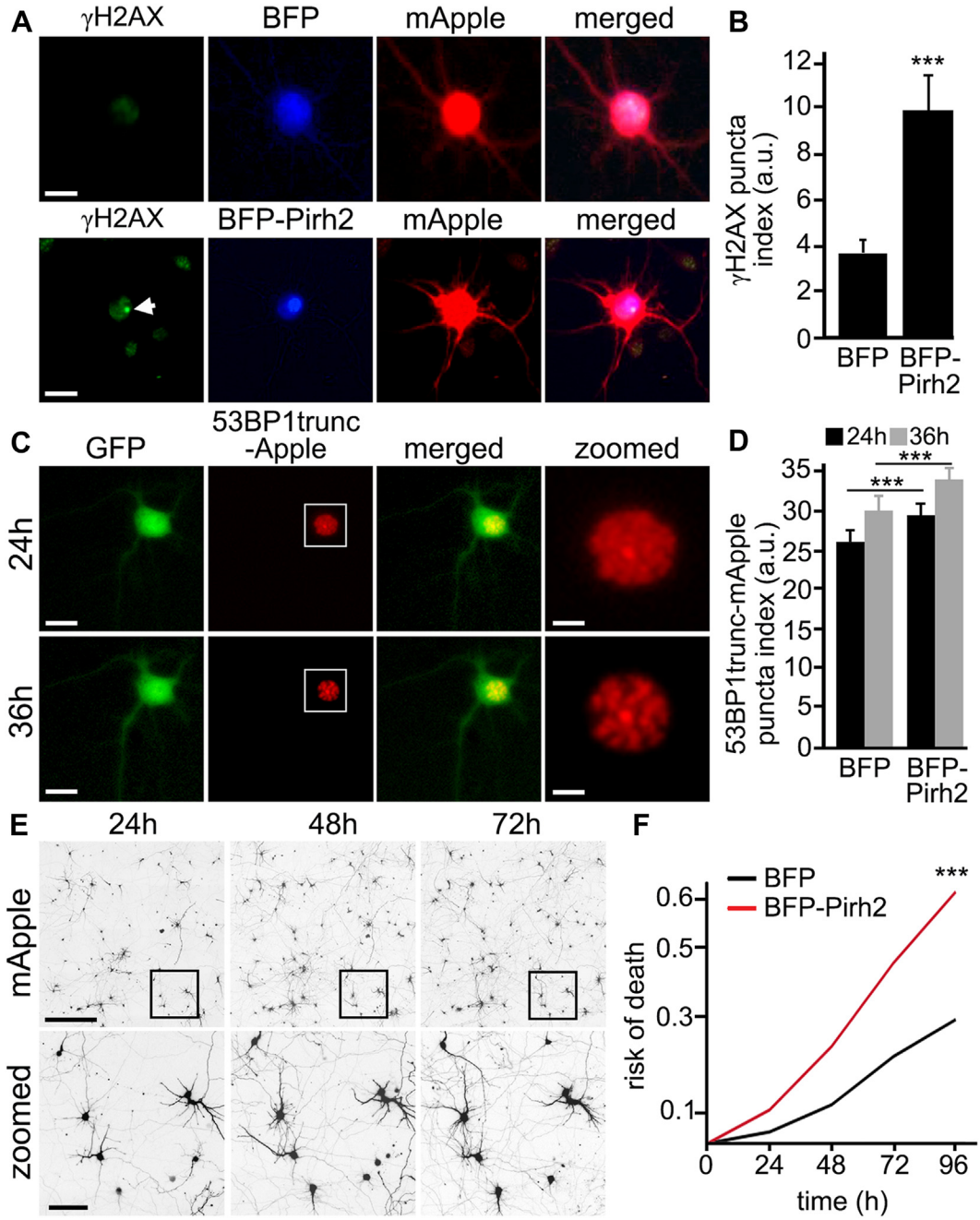

Figure 7. Pirh2 promotes DNA damage and neurodegeneration in cultured primary neurons. *A*, primary cortical neurons were transfected with BFP and mApple or with NLS-BFP-Pirh2 (BFP-Pirh2) and mApple. Cells were fixed, stained with antibodies against γH2AX, and imaged (*green*). Scale bar represents 10 μm. Note that γH2AX-positive punctum colocalizes with BFP-Pirh2-positive punctum. *B*, the puncta index of γH2AX for BFP- and NLS-BFP-Pirh2-transfected (BFP-Pirh2) neurons was analyzed from (*A*). $p = 0.0001$ (*t* test), 300 neurons were analyzed from three experiments. *C*, primary cortical neurons were cotransfected with BFP, 53BP1trunc-Apple, and GFP or with NLS-BFP-Pirh2, 53BP1trunc-Apple, and GFP (BFP-Pirh2), and imaged 24 and 36 h after transfection. Scale bar represents 20 μm. The nuclei in the *red channel* are zoomed in to demonstrate 53BP1trunc-Apple-positive puncta. Scale bar represents 2 μm. *D*, fluorescence intensities of 53BP1trunc-mApple were analyzed from (*C*). $p = 0.0001$ (*t* test), 300 neurons were analyzed from three experiments. *E*, an example of survival analysis of primary cortical neurons. Neurons were transfected with mApple (a morphology and viability marker) and tracked with an automated microscope. Scale bar represents 400 μm. A region from the original images at different time points is zoomed to demonstrate longitudinal single-cell tracking (*bottom panel*). Scale bar represents 50 μm. *F*, primary cortical neurons were transfected with BFP and mApple, or with NLS-BFP-Pirh2 (BFP-Pirh2) and mApple, and tracked with an automated microscope for several days. Risk of death curves demonstrate that overexpressed Pirh2 was neurotoxic. $p = 0.0034$ (log-rank test), 150 neurons were analyzed from three experiments. BFP, blue fluorescent protein; NLS, nuclear localization sequence.

Discussion

Our data provide strong evidence for a novel G4 structure–based mechanism of transcription and genetic instability in neuronal cells (Fig. 10). PDS, a selective G4-DNA-binding small molecule designed to form a stable complex with G4-DNA structures (65), triggers a change in transcription in cultured primary neurons. In addition to neuron-specific mechanisms (*e.g.*, learning and memory pathways), immune

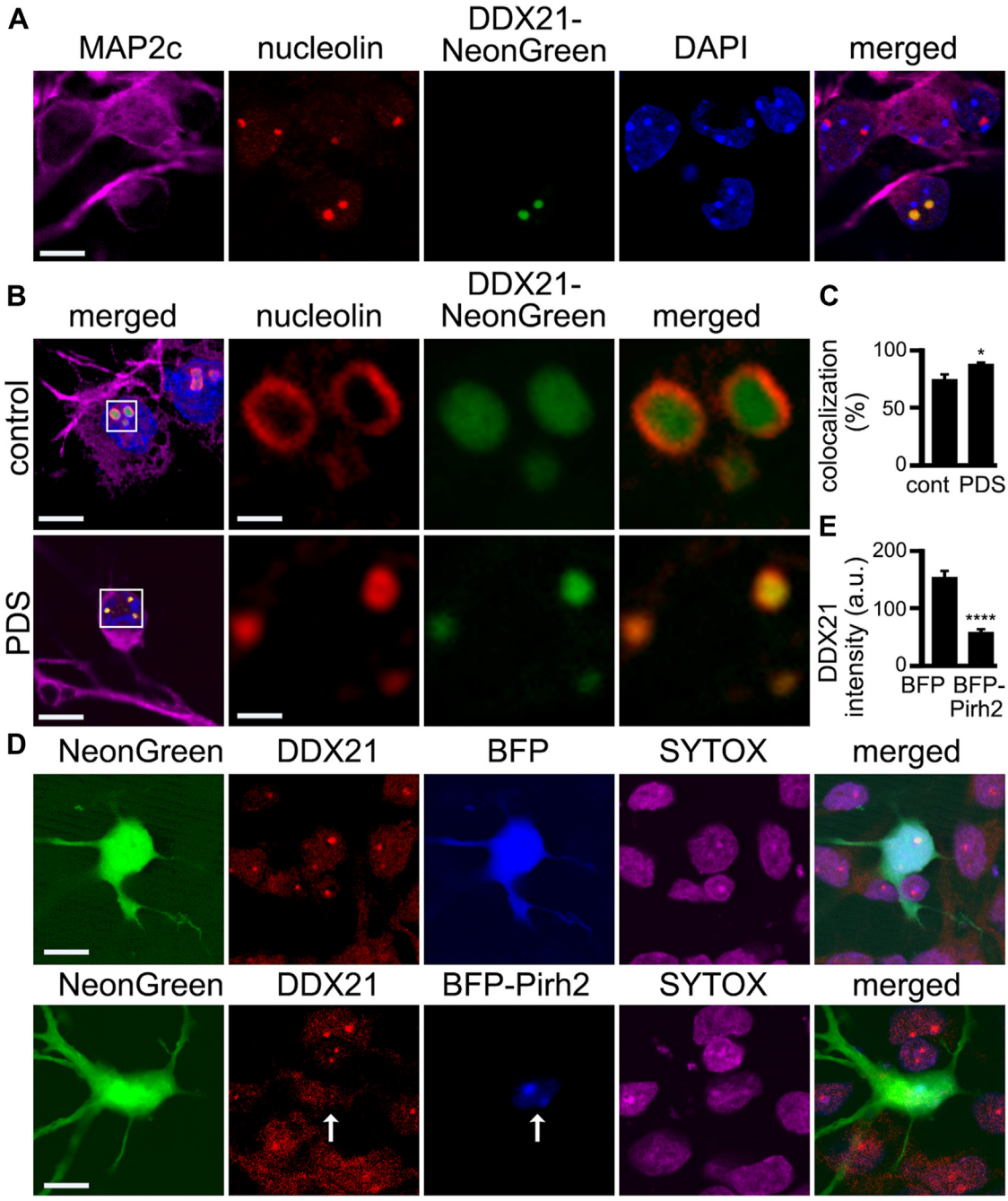

Figure 8. Pirh2 downregulates DDX21 in cultured primary neurons. *A*, primary cortical neurons were transfected with the DDX21-NeonGreen construct. Cells were fixed and stained with antibodies against nucleolin and MAP2c and the DAPI dye. Note that DDX21-NeonGreen forms puncta. Scale bar represents 5 μm. *B*, primary cortical neurons were transfected with DDX21-NeonGreen and treated with a vehicle or 2 μM pyridostatin (PDS) overnight. Cells were fixed, stained with antibodies against nucleolin and MAP2c, and imaged with a confocal microscope. The *left panel* is merged images (MAP2c, nucleolin, DDX21-NeonGreen, and DAPI). Scale bar represents 5 μm. The *right three panels* are zoomed in from the *left panel* to demonstrate that, in vehicle-treated neurons, nucleolin forms ring-like structures (the granular component of the nucleolus) and DDX21-NeonGreen forms puncta mostly within the nucleolin rings (the dense fibrillar component of the nucleolus). Note that PDS profoundly alters nucleolin- and DDX21-NeonGreen-positive foci. Scale bar represents 1 μm. *C*, colocalization of nucleolin and DDX21-NeonGreen was measured from (*B*). $p = 0.014$ (*t* test), 50 vehicle- and 50 PDS-treated neurons were analyzed from three experiments. *D*, primary cortical neurons were transfected with Neon-Green and BFP or with NeonGreen and BFP-Pirh2, fixed, and stained with antibodies against DDX21 and the SYTOX dye. Note that DDX21-positive puncta are absent in BFP-Pirh2-expressing cell (depicted with *arrow*). Scale bar represents 5 μm. *E*, fluorescence intensities of DDX21 were measured in BFP- and BFP-Pirh2-expressing neurons from (*D*). $p = 0.001$ (*t* test), 33 BFP-transfected and 44 BFP-Pirh2-transfected neurons were analyzed from three experiments. BFP, blue fluorescent protein; DAPI, 4′,6-diamidino-2-phenylindole.

response genes were altered by PDS, which was also seen in prior studies in cancer cells (20). We also discovered a novel regulator of neuronal DDRs—the E3 ubiquitin ligase Pirh2 (RCHY1), a gene that was upregulated by PDS treatment. In the nucleus, ectopically increasing Pirh2 levels promotes DNA DSBs, leading to neurotoxicity. Importantly, Pirh2 downregulates DDX21, an RNA helicase, which unfolds G4-RNA and R-loops, suggesting that accumulating R-loops may also

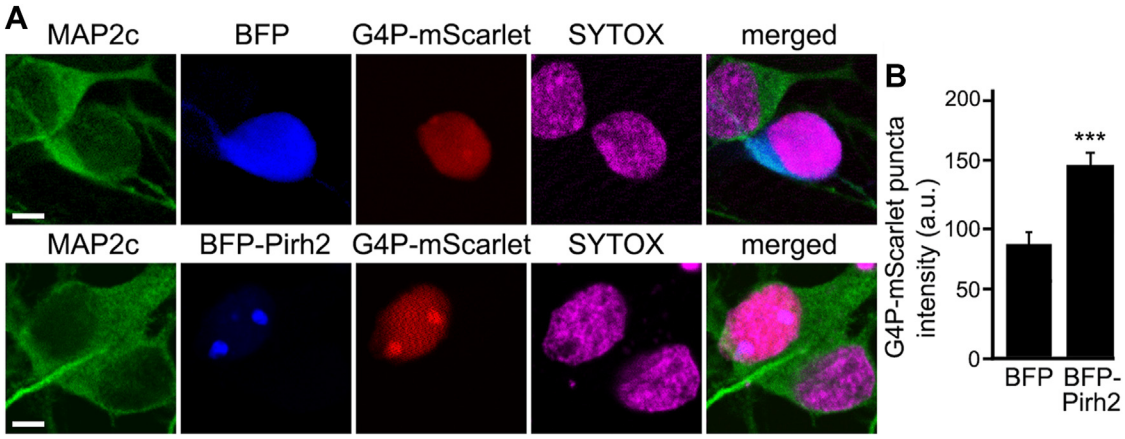

Figure 9. Pirh2 increases G4-DNA levels in the neuronal nucleolus. *A*, primary cortical neurons were transfected with BFP and the G4-DNA reporter G4P-mScarlet or with BFP-Pirh2 and G4P-mScarlet, fixed, and stained with an antibody against MAP2c and SYTOX. Note that Pirh2 increases fluorescence of the G4P-mScarlet reporter in the nucleolus. Scale bar represents 5 μm. *B*, fluorescence intensity of the G4P-mScarlet reporter in puncta was measured in BFP- and BFP-Pirh2-expressing neurons from (*A*). $p = 0.0005$ (*t* test), 63 BFP-transfected and 78 BFP-Pirh2-transfected neurons were analyzed from four experiments. BFP, blue fluorescent protein.

contribute to Pirh2-mediated DNA damage. Finally, Pirh2 promotes G4-DNA formation in the neuronal nucleolus. Thus, our results suggest that exogenous ligands (*e.g.*, G4-DNA targeting chemotherapy (19)) or lowered helicase activity (various helicase syndromes (66)) likely cause dysregulation of the entire transcriptome, leading to DNA damage, senescence, neuronal dysfunction, and neurodegeneration.

The RING finger family of E3 ubiquitin ligases is the largest of E3 ligase family and contains up to 600 members. These ligases catalyze a transfer of the ubiquitin moiety from the E2-conjugating enzymes to the substrate protein. The substrate recognition domain within an E3 ubiquitin ligase determines substrate specificity (67). The RING finger E3 ubiquitin ligase Pirh2 has at least five isoforms generated by alternative splicing (68), with the Pirh2A isoform being the full-length Pirh2 protein, which was used in our study (69). Pirh2 was originally discovered as a binding partner of the androgen receptor N-terminal interacting protein (70) and as a regulator of the androgen receptor signaling pathway, whose functions depend on Pirh2's ubiquitin ligase activity (71). Since then, several proteins have been found to interact with Pirh2. In cancerous cells, Pirh2 ubiquitinates and orchestrates the degradation of p53, p73, p27, c-Myc, COP, PolH, Chk2, HDAC1, HDAC2, and the transcription factor Twist1 (56, 72, 73). Intriguingly, it was earlier discovered that Pirh2 is a component of a protein–protein interaction network for inherited ataxias and disorders of Purkinje cell degeneration (74), suggesting that Pirh2 plays a role in neurodegenerative diseases.

A recent study showed that 225 proteins interact with Pirh2 in cancer cells, including DNA repair proteins (*e.g.*, PARP1, Ku70, DDX1, SMARCA5, and RAD18), chromatin organization proteins, transcription factors, and G4 helicases (47). Intriguingly, Pirh2 interacts with the nucleolar RNA helicase DDX21 (47), which binds G4-RNA (61), as well as other helicases (47) that bind G4-DNA or/and G4-RNA, including DHX9 (75), DDX1 (76), DDX5 (77), and DDX17 (78). Altered levels of Pirh2 have been found in brain, prostate, lung, and other cancers, with higher Pirh2 expression often being associated with poorer prognosis in many cancers (71, 79–81). Although this RING-finger E3 ubiquitin ligase modulates the degradation of a number of critical DNA repair proteins, which are involved in neurodegeneration, Pirh2 has not been studied in neurons.

The helicase DDX21 has been mostly studied in cancer (82). In cancer cells, reduction of DDX21 leads to the accumulation of R-loops and DNA DSBs (63). Enriched in the nucleolus, DDX21 regulates rRNA transcription and processing (83) and binds to and resolves G4-RNA (61). SIRT7 deacetylates DDX21 and thereby increases DDX21's helicase activity (63). DDX21 interacts with Pirh2 (47), likely indicating that DDX21 is a substrate for Pirh2. Our data revealed that, as in cancer cells, DDX21 is nucleolar in neurons. Elevated Pirh2 leads to DNA DSBs in the nucleolus and downregulation of DDX21, suggesting these two events may be connected. Since DDX21 has not been studied in neurons, our study opens a novel avenue for DDX21 research in neurodegenerative diseases.

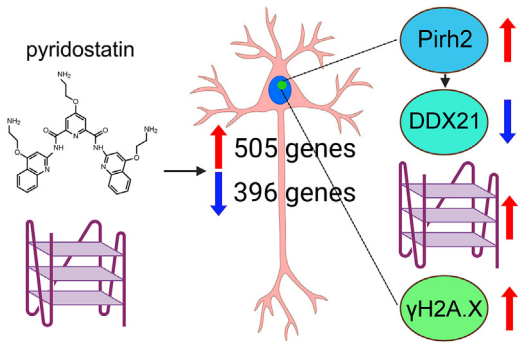

Figure 10. Model of Pirh2-dependent DNA damage in neurons induced by the G-quadruplex ligand pyridostatin (PDS). PDS alters transcription in cultured primary neurons, leading to changes in various neuron-specific and neuron-nonspecific pathways. The E3 ubiquitin ligase Pirh2 is upregulated and localizes to the nucleolus, resulting in DNA damage as evidenced by γH2AX upregulation, downregulation of the helicase DDX21, and elevated G4-DNA levels.

The nucleolus is a nuclear nonmembrane-bound structure, the site of the initial ribosome biogenesis, that contains actively transcribed rDNA, polymerases I and III, pre-rRNA, and nuclear ribonucleoprotein complexes. Intriguingly, misfolded proteins associate with the nucleolus, which possesses a chaperone-like activity, thereby facilitating refolding during recovery from stress. Continued stress leads to a loss of chaperone-like activities, nucleolar dysfunction, and cytotoxicity (84). Nucleolar protein sequestration and release also critically regulates stress responses, including DDRs. rDNA, the most transcribed DNA region, is a hot spot of DNA DSBs. For example, nucleolar stress results in the stabilization of p53, whereas recovery from stress leads to p53 ubiquitylation and proteasomal degradation (85). Although p53 is enriched in the nucleoplasm and cytoplasm, the nucleolus contains polyubiquitylated p53 that, once polyubiquitylated by the E3 ubiquitin–protein ligase MDM2, is released from the nucleolus and degraded, a process critically modulated by DNA damage, metabolic stress, and oncogenes (85). Intriguingly, there is close communication between the nucleolus and PML bodies: under stress, PML protects p53 from MDM2-mediated polyubiquitination and degradation by recruiting p53 to the PML bodies (86). These molecular mechanisms were discovered by using non-neuronal, mostly cancer cells. However, whether neurons undergo similar processes during stress is not fully understood. We demonstrate that, in neurons, Pirh2 is enriched in the nucleolus. Therefore, at least some nucleolar pathways are shared between non-neuronal and postmitotic neuronal cells.

The use of G4 ligands to stabilize G4-DNA is being investigated as a potential anticancer therapy (19, 87, 88). In cancer cells, overly stable G4-DNA structures may interfere with replication and transcription, promote DNA damage, and thereby inhibit tumor growth. PDS triggers innate immune gene activation in cancer cells, suggesting that G4-DNA ligands may function as immunomodulators in immunotherapy (20). However, we demonstrated that injecting mice with PDS results in cognitive impairment and accelerated brain aging (38). We also showed that PDS promotes chromatin restructuring and DNA damage in neurons, astrocytes, and microglia (15). Moreover, neurons are more sensitive to PDS than dividing astrocytes and microglial cells (15), highlighting important differences between post-mitotic and mitotic cells (89). Another study demonstrated that stabilizing G4 structures with PDS leads to accelerated aging in *Caenorhabditis elegans* (90). Therefore, our current study has significant ramifications for the oncology field: targeting G4-DNA in cancer cells may have an unwanted side effect of accelerated aging of healthy cells, including nonreplaceable neurons.

In cancerous MCF-7 cells, PDS upregulates 727 and downregulates 872 genes (20), numbers similar to those we observed in neuronal cells (505 genes were downregulated and 396 genes were upregulated by PDS in neurons; Fig. 1, *B* and *C*). In cancer cells, the altered gene networks included type I interferon responses, inflammatory antiviral responses, immune cell regulation, chromatin organization, mitochondrial function, and translation (20). Intriguingly, Pirh2/Rchy1 was not affected by PDS in MCF-7 cells (20), highlighting important differences between cancer cells and neurons. In our study, PDS altered numerous neuron-specific pathways (Fig. 2) and immune and inflammatory networks, similarly to cancer cells. In enrichment analysis, the p53 pathway was overrepresented in neuronal samples treated with PDS, with most genes being upregulated, including Pirh2/Rchy1 (Fig. 3). It is not clear what upregulates the p53 pathway in PDS-treated neurons: it could be altered expression of certain genes or G4- or topoisomerase II-dependent DNA damage as PDS may alter DNA topology likely by trapping topoisomerase II on DNA (16, 17, 19). Future studies will determine a molecular mechanism of Pirh2/Rchy1 upregulation in neurons as a result of PDS treatment.

Genomic maintenance is critical in the developing, developed, and aged central nervous system (CNS). During CNS development, DNA replication is one of the major drivers of genomic instability during cell division. In the developed CNS, high transcriptional, topoisomerase, and high oxidative metabolism activities lead to DNA damage. In the aged CNS, in addition to the "fatigued" DNA maintenance mechanisms (*e.g.*, DNA repair), the same mechanisms promote DNA damage as in the developed CNS. It is very likely that G4 landscapes and G4-associated mechanisms strongly depend on the age of neurons *in vivo* as well. Our findings, therefore, open a new perspective on G4-associated mechanisms in developing, mature, and aged neurons.

In our study, we demonstrated that the G4 ligand PDS induces notable changes in neuronal transcription. We also identified a novel multistep mechanism of DNA damage in neuronal cells that highlights the complexity of DNA guarding and maintenance pathways in neurons. Our findings could have broad ramifications for future therapeutic development based on the targeting of G4s in neurodegenerative diseases.

Experimental procedures

Chemicals and plasmids

Antibodies against DDX21 were from Proteintech (catalog no.: 10528-1-AP). Antibodies against Map2c were from Novus Biologicals (catalog no.: NB300-213). Antibodies against nucleolin were from Cell Signaling (catalog no.: 14574). Antibodies against γH2AX were from Millipore (JBW301; catalog no.: 05-636). Antibodies against monoubiquitinylated and polyubiquitinylated protein conjugates were from Enzo Life Sciences (catalog no.: ENZ-ABS840). Rabbit antibodies against annexin V were from Proteintech (1:500 dilution; catalog no.: 11060-1-AP). Antimouse Alexa Fluor 488-labeled (catalog no.: A11001), anti-rabbit Alexa Fluor 546-labeled (catalog no.: A11010), and antichicken Alexa Fluor 647-labeled (catalog no.: A21449) secondary antibodies were from Life Technologies. The SYTOX deep red nucleic acid stain (catalog no.: P36990) and the 4′,6-diamidino-2-phenylindole (DAPI) dye (catalog no.: 62248) were from ThermoFisher Scientific. pRP-CAG-TagBFP, pRP-CAG-3xNLS-TagBFP-mPirh2, pRP-CAG-NeonGreen, pRP-CAG-DDX21-NeonGreen, and pRP-G4P-mScarlet were cloned by VectorBuilder. The G4P

sequence was published by the Tan laboratory (64) (see Acknowledgments section). pEGFP-PML was a gift from Steven Finkbeiner (Gladstone Institutes, University of California) and was described (91). pCAG-mApple and pCAG-mApple-hTP53BP1 (1220–1709 amino acids) were described (39).

Cell cultures and transfection

Brain cortices from rat or mouse embryos (E17–18) were dissected, dissociated, and plated on 12-well tissue-culture plates (4×10^5/well). Plates were coated with poly-D-lysine (Sigma–Aldrich; catalog no.: P6407), as described (38). Primary cortical neurons were grown in Neurobasal Plus Medium (Gibco; catalog no.: 21103049) supplemented with B-27 (Gibco; catalog no.: 17504001), GlutaMAX (Gibco; catalog no.: 35050061), and penicillin–streptomycin (Gibco; catalog no.: 15140122). Mouse neurons were used for RNA-Seq. Primary cultures were transfected with Lipofectamine 2000 (ThermoFisher Scientific; catalog no.: 11668019) and a total of 1 to 2 μg of plasmid DNA per well, as described (38). Some cultures were treated with PDS (2 μM, overnight) or with a vehicle (water).

Sample preparation, library preparation, and sequencing

RNA was isolated using the RNeasy Mini (QIAGEN) according to the manufacturer's instructions with an elution volume of 50 μl. The library preparation was done using the QIAseq Stranded Total RNA Library Kit with QIAseq FastSelect rRNA and globin depletion. An amount of 500 ng of starting material was heat fragmented. After first- and second-strand synthesis, the complementary DNA was end-repaired and 3′ adenylated. Sequencing adapters were ligated to the overhangs. Adapted molecules were enriched by using 13 cycles or PCR and purified by a bead-based clean-up. Library preparation was quality controlled using capillary electrophoresis (Agilent DNA 1000 Chip). High-quality libraries were pooled from equimolar concentrations. The library pool(s) were quantified using qPCR, and optimal concentration of the library pool was used to generate the clusters on the surface of a flowcell before sequencing on a NextSeq (Illumina, Inc) instrument (1×75, 2×8) according to the manufacturer instructions (Illumina, Inc).

RNA-Seq data analyses

RNA-Seq data were analyzed with iPathwayGuide (Advaita Bioinformatics) in the context of pathways obtained from the KEGG database (43, 44) and gene ontologies from the GO Consortium database (45). The underlying pathway topologies, composed of genes and their directional interactions, were obtained from the KEGG database using iPathwayGuide.

qRT–PCR

Total RNA was extracted from primary cultures using the RNeasy Mini kit (QIAGEN; catalog no.: 74104) and then reverse transcribed using iScript Reverse Transcription SuperMix (Bio-Rad; catalog no.: 1708840), according to the manufacturer's protocol and as described (38, 39). RT–qPCR was performed using a Bio-Rad CFX96 Touch machine using SSoAdvanced Universal SYBR Green (Bio-Rad; catalog no.: 1725275) for visualization and quantification according to the manufacturer's instructions. Primer sequences were ATG7 (Atg7), forward: 5′-TCCTGAGAGCATCCCTCTAATC-3′, reverse: 5′-CTTCAGTTCGACACAGGTCATC-3′; TBP (Tbp), forward: 5′-AGTGCCCAGCATCACTGTTT-3′, reverse: 5′-GGTCCATGACTCTCACTTTCTT-3′, BRCA1 (Brca1), forward: 5′-GCAGATGGGCTGACAGTAAA-3′, reverse: 5′-GCTTTCTACCACAGAGGGAATC-3′, Pirh2 (Pirh2), forward: 5′-GCCTAACCACGAATCTTCGAGG-3′; reverse: 5′-ACACGGCAAGACGTGAGCAACA-3′. The PCR conditions were 95 °C for 3 min, followed by 40 cycles of 95 °C for 10 s and 55 °C for 30 s. Relative expression levels were calculated from the average threshold cycle number using the delta–delta Ct method.

Fluorescence microscopy and image analysis

Living or fixed cells in 24-well plates were imaged using the automated EVOS microscopy system (ThermoFisher Scientific). The microscope was set to image 5% of the center of the well area with the 20× objective and to capture the red fluorescent protein, GFP, and DAPI signal. Neurons were also imaged with the Leica DMi8 confocal with the 63× ACS APO 63×/1.30 oil lens. Images were subsequently analyzed with the ImageJ/Fiji software. Colocalization of fluorescent signals was measured with the EzColocalization plugin for ImageJ/Fiji (92). γH2A.X fluorescence was analyzed by the puncta index, which is the standard deviation of the intensities measured among pixels within a region of interest. Low puncta index represents diffuse localization, whereas a high puncta index represents punctate localization. All assessments were performed by a blinded investigator.

Survival analysis

Neuronal survival was determined by using an automated microscopy and longitudinal analysis. This method allows us to track large cohorts of neurons and to sensitively measure their survival with the statistical analyses used in clinical medicine (59). Neurons were transfected with a survival and morphology marker (mApple) and a protein of interest (3xNLS-TagBFP-mPirh2). Neurons were imaged at 24 h after transfection and then every 24 h for 4 days. The plate with cells was placed on the microscope stage, which automatically positions the 20× objective to the center of a well. The microscope system takes fluorescence images of the center area of the well by moving the stage to each adjacent field in the well. For tracking the same group of cells over time, an image of the fiduciary field on the plate was collected at the first time point and used as a reference image. Neurons that died during the imaging interval were assigned a survival time. These events were transformed into log values and plotted in risk of death curves and analyzed for statistical significance (log-rank test). JMP software (SAS Institute) was used to analyze data and generate survival curves (38).

Immunocytochemistry

Cultured primary neurons from rat or mouse embryos of both sexes were grown on coverslips. Neurons were washed with PBS and fixed with 4% paraformaldehyde–PBS solution for 15 min at room temperature. Cells were rinsed and incubated with 0.1% Triton X-100–PBS solution for 5 min at room temperature to permeabilize membranes. Cells were then rinsed with PBS and incubated with 1% bovine serum albumin–PBS solution for 1 h at room temperature. Cells were incubated with a primary antibody overnight at 4 °C, washed, and incubated with a secondary antibody for 1 h at room temperature. Coverslips were mounted with the SYTOX deep red nucleic acid dye or the DAPI dye before imaging.

G4-DNA analyses

The QGRS mapper (http://bioinformatics.ramapo.edu/QGRS/analyze.php) was used to determine the potential G4-DNA structures contained in the Pirh2 gene and its promoter. Search parameters for the QGRS mapper were maximal length: 45; minimal G-group size: 3; and loop size: from 0 to 10 (6, 93).

Statistical analyses

The statistical analyses and tests were performed with ImageJ and GraphPad Prism (GraphPad Software, Inc) software.

Ethical approval

Rats and mice were maintained in accordance with guidelines and regulations of the University of Texas McGovern Medical School at Houston. All experimental protocols were approved by the University of Texas McGovern Medical School at Houston. The methods were carried out in accordance with the approved guidelines.

Data availability

Data are available within the article or its supporting information.

Supporting information—This article contains supporting information.

Acknowledgments—We thank Zheng Tan for allowing the use the G4P protein (64) in our studies. We thank members of the A. S. T. laboratory and the BRAINS laboratory for useful discussions. We also thank Megan Taylor (bioinformatics scientist, genomic services, QIAGEN) and Suresh Kumar (bioinformatics scientist, Advaita Bioinformatics) for helpful discussions. Nur Compan and Danielle Guillory provided administrative assistance. The Leica DMi8 confocal microscope is supported in part by the Huffington Foundation.

Author contributions—A. U., S. P. M., N. K., D. M., and L. D. M. conceptualization; A. S. T. methodology; R. D. E., J. F. M.-M., and A. S. T. formal analysis; R. D. E., A. A. P., and J. F. M.-M. data curation; A. S. T. writing–original draft; R. D. E., J. F. M.-M., A. U., S. P. M., N. K., D. M., L. D. M., and A. S. T. writing–review & editing; A. U., S. P. M., and A. S. T. funding acquisition.

Funding and additional information—This work was supported by the Hereditary Disease Foundation (to J. F. M.-M.), the National Institute on Aging (grant no.: 1RF1AG068292) (to A. S. T., S. P. M., and A. U.), and by the Glenn Foundation and the American Federation for Aging Research (grant no.: BIG21042) (to A. S. T.).

Conflict of interest—The authors declare that they have no conflicts of interest with the contents of this article.

Abbreviations—The abbreviations used are: BFP, blue fluorescent protein; CNS, central nervous system; DAPI, 4′,6-diamidino-2-phenylindole; DDR, DNA damage response; DIV, days *in vitro*; DSB, double-strand break; G4, G-quadruplex; GO, Gene Ontology; KEGG, Kyoto Encyclopedia of Genes and Genomes; NLS, nuclear localization sequence; PCA, principal component analysis; PDS, pyridostatin; PML, promyelocytic leukemia; QFS, G4-forming sequence; qPCR, quantitative PCR; rDNA, ribosomal DNA.

References

1. Lane, A. N., Chaires, J. B., Gray, R. D., and Trent, J. O. (2008) Stability and kinetics of G-quadruplex structures. *Nucleic Acids Res.* **36**, 5482–5515
2. Meier-Stephenson, V. (2022) G4-quadruplex-binding proteins: review and insights into selectivity. *Biophys. Rev.* **14**, 635–654
3. Sauer, M., and Paeschke, K. (2017) G-quadruplex unwinding helicases and their function *in vivo*. *Biochem. Soc. Trans.* **45**, 1173–1182
4. Lejault, P., Mitteaux, J., Sperti, F. R., and Monchaud, D. (2021) How to untie G-quadruplex knots and why? *Cell Chem. Biol.* **28**, 436–455
5. Rhodes, D., and Lipps, H. J. (2015) G-quadruplexes and their regulatory roles in biology. *Nucleic Acids Res.* **43**, 8627–8637
6. Maizels, N., and Gray, L. T. (2013) The G4 genome. *PLoS Genet.* **9**, e1003468
7. Puig Lombardi, E., and Londoño-Vallejo, A. (2019) A guide to computational methods for G-quadruplex prediction. *Nucleic Acids Res.* **48**, 1–15
8. Chambers, V. S., Marsico, G., Boutell, J. M., Di Antonio, M., Smith, G. P., and Balasubramanian, S. (2015) High-throughput sequencing of DNA G-quadruplex structures in the human genome. *Nat. Biotechnol.* **33**, 877–881
9. Marsico, G., Chambers, V. S., Sahakyan, A. B., McCauley, P., Boutell, J. M., Antonio, M. D., *et al.* (2019) Whole genome experimental maps of DNA G-quadruplexes in multiple species. *Nucleic Acids Res.* **47**, 3862–3874
10. Besnard, E., Babled, A., Lapasset, L., Milhavet, O., Parrinello, H., Dantec, C., *et al.* (2012) Unraveling cell type-specific and reprogrammable human replication origin signatures associated with G-quadruplex consensus motifs. *Nat. Struct. Mol. Biol.* **19**, 837–844
11. Damas, J., Carneiro, J., Goncalves, J., Stewart, J. B., Samuels, D. C., Amorim, A., *et al.* (2012) Mitochondrial DNA deletions are associated with non-B DNA conformations. *Nucleic Acids Res.* **40**, 7606–7621
12. Spiegel, J., Cuesta, S. M., Adhikari, S., Hänsel-Hertsch, R., Tannahill, D., and Balasubramanian, S. (2021) G-quadruplexes are transcription factor binding hubs in human chromatin. *Genome Biol.* **22**, 117
13. Hansel-Hertsch, R., Beraldi, D., Lensing, S. V., Marsico, G., Zyner, K., Parry, A., *et al.* (2016) G-quadruplex structures mark human regulatory chromatin. *Nat. Genet.* **48**, 1267–1272
14. Biffi, G., Tannahill, D., Miller, J., Howat, W. J., and Balasubramanian, S. (2014) Elevated levels of G-quadruplex formation in human stomach and liver cancer tissues. *PLoS One* **9**, e102711
15. Tabor, N., Ngwa, C., Mitteaux, J., Meyer, M. D., Moruno-Manchon, J. F., Zhu, L., *et al.* (2021) Differential responses of neurons, astrocytes, and microglia to G-quadruplex stabilization. *Aging (Albany NY)* **13**, 15917–15941

16. Rodriguez, R., Miller, K. M., Forment, J. V., Bradshaw, C. R., Nikan, M., Britton, S., *et al.* (2012) Small-molecule–induced DNA damage identifies alternative DNA structures in human genes. *Nat. Chem. Biol.* **8**, 301–310
17. Olivieri, M., Cho, T., Álvarez-Quilón, A., Li, K., Schellenberg, M. J., Zimmermann, M., *et al.* (2020) A genetic map of the response to DNA damage in human cells. *Cell* **182**, 481–496.e421
18. Bossaert, M., Pipier, A., Riou, J.-F., Noirot, C., Nguyên, L.-T., Serre, R.-F., *et al.* (2021) Transcription-associated topoisomerase 2α (TOP2A) activity is a major effector of cytotoxicity induced by G-quadruplex ligands. *Elife* **10**, e65184
19. Zell, J., Rota Sperti, F., Britton, S., and Monchaud, D. (2021) DNA folds threaten genetic stability and can be leveraged for chemotherapy. *RSC Chem. Biol.* **2**, 47–76
20. Miglietta, G., Russo, M., Duardo, R. C., and Capranico, G. (2021) G-quadruplex binders as cytostatic modulators of innate immune genes in cancer cells. *Nucleic Acids Res.* **49**, 6673–6686
21. Maynard, S., Fang, E. F., Scheibye-Knudsen, M., Croteau, D. L., and Bohr, V. A. (2015) DNA damage, DNA repair, aging, and neurodegeneration. *Cold Spring Harb. Perspect. Med.* **5**, a025130
22. Suberbielle, E., Sanchez, P. E., Kravitz, A. V., Wang, X., Ho, K., Eilertson, K., *et al.* (2013) Physiologic brain activity causes DNA double-strand breaks in neurons, with exacerbation by amyloid-beta. *Nat. Neurosci.* **16**, 613–621
23. Madabhushi, R., Pan, L., and Tsai, L. H. (2014) DNA damage and its links to neurodegeneration. *Neuron* **83**, 266–282
24. Canugovi, C., Misiak, M., Ferrarelli, L. K., Croteau, D. L., and Bohr, V. A. (2013) The role of DNA repair in brain related disease pathology. *DNA Repair* **12**, 578–587
25. Penndorf, D., Witte, O., and Kretz, A. (2018) DNA plasticity and damage in amyotrophic lateral sclerosis. *Neural Regen. Res.* **13**, 173–180
26. Katapadi, V. K., Nambiar, M., and Raghavan, S. C. (2012) Potential G-quadruplex formation at breakpoint regions of chromosomal translocations in cancer may explain their fragility. *Genomics* **100**, 72–80
27. Wiedemann, E.-M., Peycheva, M., and Pavri, R. (2016) DNA replication origins in immunoglobulin switch regions regulate class switch recombination in an r-loop-dependent manner. *Cell Rep.* **17**, 2927–2942
28. Ribeyre, C., Lopes, J., Boule, J. B., Piazza, A., Guedin, A., Zakian, V. A., *et al.* (2009) The yeast Pif1 helicase prevents genomic instability caused by G-quadruplex-forming CEB1 sequences *in vivo*. *PLoS Genet.* **5**, e1000475
29. Piazza, A., Largy, E., Boulé, J.-B., Lopes, J., Mingo, K., Teulade-Fichou, M.-P., *et al.* (2010) Genetic instability triggered by G-quadruplex interacting Phen-DC compounds in Saccharomyces cerevisiae. *Nucleic Acids Res.* **38**, 4337–4348
30. Massey, T. H., and Jones, L. (2018) The central role of DNA damage and repair in CAG repeat diseases. *Dis. Model. Mech.* **11**, dmm031930
31. Puget, N., Miller, K. M., and Legube, G. (2019) Non-canonical DNA/RNA structures during transcription-coupled double-strand break repair: roadblocks or bona fide repair intermediates? *DNA Repair (Amst)* **81**, 102661
32. Bruno, P. M., Lu, M., Dennis, K. A., Inam, H., Moore, C. J., Sheehe, J., *et al.* (2020) The primary mechanism of cytotoxicity of the chemotherapeutic agent CX-5461 is topoisomerase II poisoning. *Proc. Natl. Acad. Sci. U. S. A.* **117**, 4053–4060
33. Paeschke, K., Bochman, M. L., Garcia, P. D., Cejka, P., Friedman, K. L., Kowalczykowski, S. C., *et al.* (2013) Pif1 family helicases suppress genome instability at G-quadruplex motifs. *Nature* **497**, 458–462
34. Yadav, P., Owiti, N., and Kim, N. (2016) The role of topoisomerase I in suppressing genome instability associated with a highly transcribed guanine-rich sequence is not restricted to preventing RNA:DNA hybrid accumulation. *Nucleic Acids Res.* **44**, 718–729
35. Lopez, C. R., Singh, S., Hambarde, S., Griffin, W. C., Gao, J., Chib, S., *et al.* (2017) Yeast Sub1 and human PC4 are G-quadruplex binding proteins that suppress genome instability at co-transcriptionally formed G4 DNA. *Nucleic Acids Res.* **45**, 5850–5862
36. Clynes, D., Jelinska, C., Xella, B., Ayyub, H., Scott, C., Mitson, M., *et al.* (2015) Suppression of the alternative lengthening of telomere pathway by the chromatin remodelling factor ATRX. *Nat. Commun.* **6**, 7538
37. Wang, Y., Yang, J., Wild, A. T., Wu, W. H., Shah, R., Danussi, C., *et al.* (2019) G-quadruplex DNA drives genomic instability and represents a targetable molecular abnormality in ATRX-deficient malignant glioma. *Nat. Commun.* **10**, 943
38. Moruno-Manchon, J. F., Lejault, P., Wang, Y., McCauley, B., Honarpisheh, P., Morales Scheihing, D. A., *et al.* (2020) Small-molecule G-quadruplex stabilizers reveal a novel pathway of autophagy regulation in neurons. *Elife* **9**, e52283
39. Moruno-Manchon, J. F., Koellhoffer, E. C., Gopakumar, J., Hambarde, S., Kim, N., McCullough, L. D., *et al.* (2017) The G-quadruplex DNA stabilizing drug pyridostatin promotes DNA damage and downregulates transcription of Brca1 in neurons. *Aging (Albany NY)* **9**, 1957–1970
40. Vijay Kumar, M. J., Morales, R., and Tsvetkov, A. S. (2023) G-quadruplexes and associated proteins in aging and Alzheimer's disease. *Front. Aging* **4**, 1164057
41. Duquette, M. L., Handa, P., Vincent, J. A., Taylor, A. F., and Maizels, N. (2004) Intracellular transcription of G-rich DNAs induces formation of G-loops, novel structures containing G4 DNA. *Genes Dev.* **18**, 1618–1629
42. Miglietta, G., Russo, M., and Capranico, G. (2020) G-quadruplex–R-loop interactions and the mechanism of anticancer G-quadruplex binders. *Nucleic Acids Res.* **48**, 11942–11957
43. Kanehisa, M., and Goto, S. (2000) KEGG: kyoto encyclopedia of genes and genomes. *Nucleic Acids Res.* **28**, 27–30
44. Kanehisa, M., Goto, S., Kawashima, S., and Nakaya, A. (2002) The KEGG databases at GenomeNet. *Nucleic Acids Res.* **30**, 42–46
45. Ashburner, M., Ball, C. A., Blake, J. A., Botstein, D., Butler, H., Cherry, J. M., *et al.* (2000) Gene ontology: tool for the unification of biology. The gene ontology consortium. *Nat. Genet.* **25**, 25–29
46. Kastenhuber, E. R., and Lowe, S. W. (2017) Putting p53 in context. *Cell* **170**, 1062–1078
47. Daks, A., Petukhov, A., Fedorova, O., Shuvalov, O., Kizenko, A., Tananykina, E., *et al.* (2021) The RNA-binding protein HuR is a novel target of Pirh2 E3 ubiquitin ligase. *Cell Death Dis.* **12**, 581
48. Logan, I. R., Sapountzi, V., Gaughan, L., Neal, D. E., and Robson, C. N. (2004) Control of human PIRH2 protein stability: involvement of TIP60 and the proteosome. *J. Biol. Chem.* **279**, 11696–11704
49. Wang, Z., Yang, B., Dong, L., Peng, B., He, X., and Liu, W. (2011) A novel oncoprotein Pirh2: rising from the shadow of MDM2. *Cancer Sci.* **102**, 909–917
50. Chen, M., Cortay, J. C., Logan, I. R., Sapountzi, V., Robson, C. N., and Gerlier, D. (2005) Inhibition of ubiquitination and stabilization of human ubiquitin E3 ligase PIRH2 by measles virus phosphoprotein. *J. Virol.* **79**, 11824–11836
51. Hattori, T., Isobe, T., Abe, K., Kikuchi, H., Kitagawa, K., Oda, T., *et al.* (2007) Pirh2 promotes ubiquitin-dependent degradation of the cyclin-dependent kinase inhibitor p27Kip1. *Cancer Res.* **67**, 10789–10795
52. Corcoran, C. A., Montalbano, J., Sun, H., He, Q., Huang, Y., and Sheikh, M. S. (2009) Identification and characterization of two novel isoforms of Pirh2 ubiquitin ligase that negatively regulate p53 independent of RING finger domains. *J. Biol. Chem.* **284**, 21955–21970
53. Lallemand-Breitenbach, V., and de Thé, H. (2018) PML nuclear bodies: from architecture to function. *Curr. Opin. Cell Biol.* **52**, 154–161
54. Boisvert, F.-M., van Koningsbruggen, S., Navascués, J., and Lamond, A. I. (2007) The multifunctional nucleolus. *Nat. Rev. Mol. Cell Biol.* **8**, 574–585
55. Imrichova, T., Hubackova, S., Kucerova, A., Kosla, J., Bartek, J., Hodny, Z., *et al.* (2019) Dynamic PML protein nucleolar associations with persistent DNA damage lesions in response to nucleolar stress and senescence-inducing stimuli. *Aging (Albany NY)* **11**, 7206–7235
56. Halaby, M. J., Hakem, R., and Hakem, A. (2013) Pirh2: an E3 ligase with central roles in the regulation of cell cycle, DNA damage response, and differentiation. *Cell Cycle* **12**, 2733–2737
57. Bonner, W. M., Redon, C. E., Dickey, J. S., Nakamura, A. J., Sedelnikova, O. A., Solier, S., *et al.* (2008) γH2AX and cancer. *Nat. Rev. Cancer* **8**, 957–967
58. Yang, K. S., Kohler, R. H., Landon, M., Giedt, R., and Weissleder, R. (2015) Single cell resolution *in vivo* imaging of DNA damage following PARP inhibition. *Sci. Rep.* **5**, 10129

59. Arrasate, M., and Finkbeiner, S. (2005) Automated microscope system for determining factors that predict neuronal fate. *Proc. Natl. Acad. Sci. U. S. A.* **102**, 3840–3845
60. McRae, E. K. S., Dupas, S. J., Booy, E. P., Piragasam, R. S., Fahlman, R. P., and McKenna, S. A. (2020) An RNA guanine quadruplex regulated pathway to TRAIL-sensitization by DDX21. *RNA* **26**, 44–57
61. McRae, E. K. S., Booy, E. P., Moya-Torres, A., Ezzati, P., Stetefeld, J., and McKenna, S. A. (2017) Human DDX21 binds and unwinds RNA guanine quadruplexes. *Nucleic Acids Res.* **45**, 6656–6668
62. Lyu, J., Shao, R., Kwong Yung, P. Y., and Elsässer, S. J. (2021) Genome-wide mapping of G-quadruplex structures with CUT&Tag. *Nucleic Acids Res.* **50**, e13
63. Song, C., Hotz-Wagenblatt, A., Voit, R., and Grummt, I. (2017) SIRT7 and the DEAD-box helicase DDX21 cooperate to resolve genomic R loops and safeguard genome stability. *Genes Dev.* **31**, 1370–1381
64. Zheng, K. W., Zhang, J. Y., He, Y. D., Gong, J. Y., Wen, C. J., Chen, J. N., *et al.* (2020) Detection of genomic G-quadruplexes in living cells using a small artificial protein. *Nucleic Acids Res.* **48**, 11706–11720
65. Rodriguez, R., Muller, S., Yeoman, J. A., Trentesaux, C., Riou, J. F., and Balasubramanian, S. (2008) A novel small molecule that alters shelterin integrity and triggers a DNA-damage response at telomeres. *J. Am. Chem. Soc.* **130**, 15758–15759
66. Brosh, R. M., and Matson, S. W. (2020) History of DNA helicases. *Genes(Basel)* **11**, 255
67. Lipkowitz, S., and Weissman, A. M. (2011) RINGs of good and evil: RING finger ubiquitin ligases at the crossroads of tumour suppression and oncogenesis. *Nat. Rev. Cancer* **11**, 629–643
68. Jung, Y. S., Qian, Y., and Chen, X. (2012) Pirh2 RING-finger E3 ubiquitin ligase: its role in tumorigenesis and cancer therapy. *FEBS Lett.* **586**, 1397–1402
69. Niazi, S., Purohit, M., and Niazi, J. H. (2018) Role of p53 circuitry in tumorigenesis: a brief review. *Eur. J. Med. Chem.* **158**, 7–24
70. Beitel, L. K., Elhaji, Y. A., Lumbroso, R., Wing, S. S., Panet-Raymond, V., Gottlieb, B., *et al.* (2002) Cloning and characterization of an androgen receptor N-terminal-interacting protein with ubiquitin-protein ligase activity. *J. Mol. Endocrinol.* **29**, 41–60
71. Logan, I. R., Gaughan, L., McCracken, S. R., Sapountzi, V., Leung, H. Y., and Robson, C. N. (2006) Human PIRH2 enhances androgen receptor signaling through inhibition of histone deacetylase 1 and is overexpressed in prostate cancer. *Mol. Cell. Biol.* **26**, 6502–6510
72. Choi, M., Choi, Y. M., An, I. S., Bae, S., Jung, J. H., and An, S. (2020) E3 ligase RCHY1 negatively regulates HDAC2. *Biochem. Biophys. Res. Commun.* **521**, 37–41
73. Yang-Hartwich, Y., Tedja, R., Roberts, C. M., Goodner-Bingham, J., Cardenas, C., Gurea, M., *et al.* (2019) p53-Pirh2 complex promotes Twist1 degradation and inhibits EMT. *Mol. Cancer Res.* **17**, 153–164
74. Lim, J., Hao, T., Shaw, C., Patel, A. J., Szabó, G., Rual, J. F., *et al.* (2006) A protein-protein interaction network for human inherited ataxias and disorders of Purkinje cell degeneration. *Cell* **125**, 801–814
75. Murat, P., Marsico, G., Herdy, B., Ghanbarian, A., Portella, G., and Balasubramanian, S. (2018) RNA G-quadruplexes at upstream open reading frames cause DHX36- and DHX9-dependent translation of human mRNAs. *Genome Biol.* **19**, 229
76. Ribeiro de Almeida, C., Dhir, S., Dhir, A., Moghaddam, A. E., Sattentau, Q., Meinhart, A., *et al.* (2018) RNA helicase DDX1 Converts RNA G-quadruplex structures into R-loops to promote IgH class switch recombination. *Mol. Cell* **70**, 650–662.e658
77. Wu, G., Xing, Z., Tran, E. J., and Yang, D. (2019) DDX5 helicase resolves G-quadruplex and is involved in MYC gene transcriptional activation. *Proc. Natl. Acad. Sci. U. S. A.* **116**, 20453–20461
78. Mestre-Fos, S., Penev, P. I., Suttapitugsakul, S., Hu, M., Ito, C., Petrov, A. S., *et al.* (2019) G-quadruplexes in human ribosomal RNA. *J. Mol. Biol.* **431**, 1940–1955
79. Daks, A., Petukhov, A., Fedorova, O., Shuvalov, O., Merkulov, V., Vasileva, E., *et al.* (2016) E3 ubiquitin ligase Pirh2 enhances tumorigenic properties of human non-small cell lung carcinoma cells. *Genes Cancer* **7**, 383–393
80. Bao, Y., Wu, X., Yuan, D., Shi, W., and Shi, J. (2017) High expression of Pirh2 is associated with poor prognosis in glioma. *Cell. Mol. Neurobiol.* **37**, 1501–1509
81. Yang, S., Chen, Y., Sun, F., Ni, Q., Wang, H., Huang, Y., *et al.* (2016) Downregulated PIRH2 can decrease the proliferation of breast cancer cells. *Arch. Med. Res.* **47**, 186–195
82. Cargill, M., Venkataraman, R., and Lee, S. (2021) DEAD-box RNA helicases and genome stability. *Genes (Basel)* **12**, 1471
83. Calo, E., Flynn, R. A., Martin, L., Spitale, R. C., Chang, H. Y., and Wysocka, J. (2015) RNA helicase DDX21 coordinates transcription and ribosomal RNA processing. *Nature* **518**, 249–253
84. Frottin, F., Schueder, F., Tiwary, S., Gupta, R., Körner, R., Schlichthaerle, T., *et al.* (2019) The nucleolus functions as a phase-separated protein quality control compartment. *Science* **365**, 342–347
85. Boyd, M. T., Vlatkovic, N., and Rubbi, C. P. (2011) The nucleolus directly regulates p53 export and degradation. *J. Cell Biol.* **194**, 689–703
86. Louria-Hayon, I., Grossman, T., Sionov, R. V., Alsheich, O., Pandolfi, P. P., and Haupt, Y. (2003) The promyelocytic leukemia protein protects p53 from Mdm2-mediated inhibition and degradation. *J. Biol. Chem.* **278**, 33134–33141
87. Mergny, J. L., and Sen, D. (2019) DNA quadruple helices in nanotechnology. *Chem. Rev.* **119**, 6290–6325
88. Neidle, S. (2016) Quadruplex nucleic acids as novel therapeutic targets. *J. Med. Chem.* **59**, 5987–6011
89. Iyama, T., and Wilson, D. M., 3rd. (2013) DNA repair mechanisms in dividing and non-dividing cells. *DNA Repair* **12**, 620–636
90. Scheibye-Knudsen, M., Tseng, A., Borch Jensen, M., Scheibye-Alsing, K., Fang, E. F., Iyama, T., *et al.* (2016) Cockayne syndrome group A and B proteins converge on transcription-linked resolution of non-B DNA. *Proc. Natl. Acad. Sci. U. S. A.* **113**, 12502–12507
91. Korb, E., Wilkinson, C. L., Delgado, R. N., Lovero, K. L., and Finkbeiner, S. (2013) Arc in the nucleus regulates PML-dependent GluA1 transcription and homeostatic plasticity. *Nat. Neurosci.* **16**, 874–883
92. Stauffer, W., Sheng, H., and Lim, H. N. (2018) EzColocalization: an ImageJ plugin for visualizing and measuring colocalization in cells and organisms. *Sci. Rep.* **8**, 15764
93. Huppert, J. L., and Balasubramanian, S. (2005) Prevalence of quadruplexes in the human genome. *Nucleic Acids Res.* **33**, 2908–2916